
Figures and figure supplements

Hierarchical organization of context in the hippocampal episodic code

Susumu Takahashi

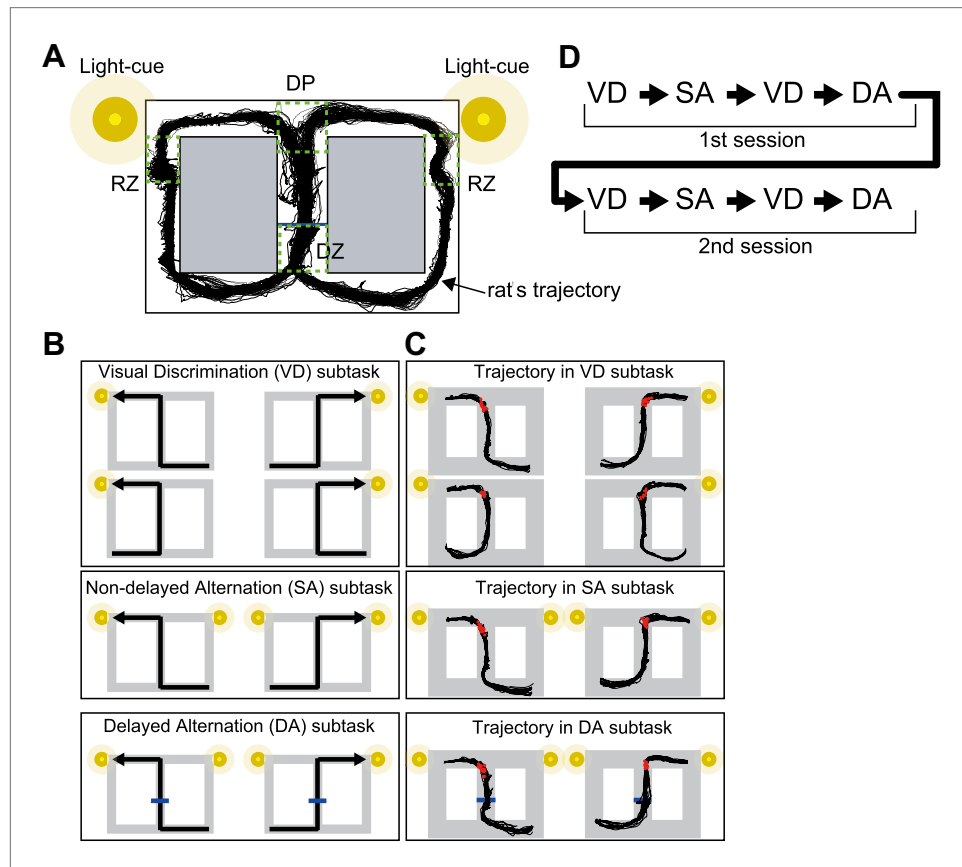


Figure 1. Task configuration. **(A)** The rat has to decide which direction to turn at the decision point (DP). If correct, the rat gets reward signals (MFB stimulations) at one of the reward zones (RZ). In the DA subtask, a barrier appears for 5 s in the central stem (blue line) so that the rat has to wait in the delay zone (DZ). An example of a running trajectory of a rat (G111125) is superimposed on the maze. **(B)** Possible journeys for three subtasks. For the VD subtask, one of the light cues is illuminated to indicate a direction. For the memory-guided (SA and DA) subtasks, both of the light cues are illuminated to alternate the direction based on memory. **(C)** Examples of running trajectories of the rat (G111125). The red dots indicate the location of the onset of the estimated turn for each lap. **(D)** The subtask sequence in a task. Each subtask consisted of 20 laps, except the second VD subtask in each session, which only consisted of 10 laps.

DOI: [10.7554/eLife.00321.003](https://doi.org/10.7554/eLife.00321.003)

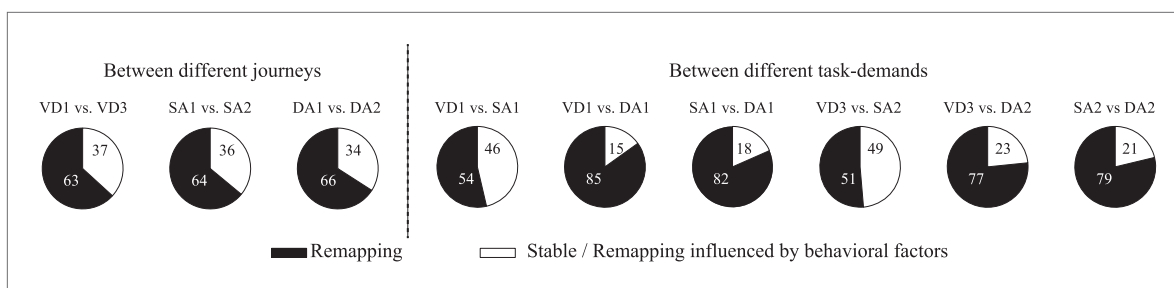


Figure 2. Proportion of differentially firing place cells. The proportion of place cells showing significantly different firing rates between different journeys within a given subtask and between different task-demands within a journey when running speed, head direction and lateral position were taken into account. Numbers indicate percentages.

DOI: [10.7554/eLife.00321.005](https://doi.org/10.7554/eLife.00321.005)

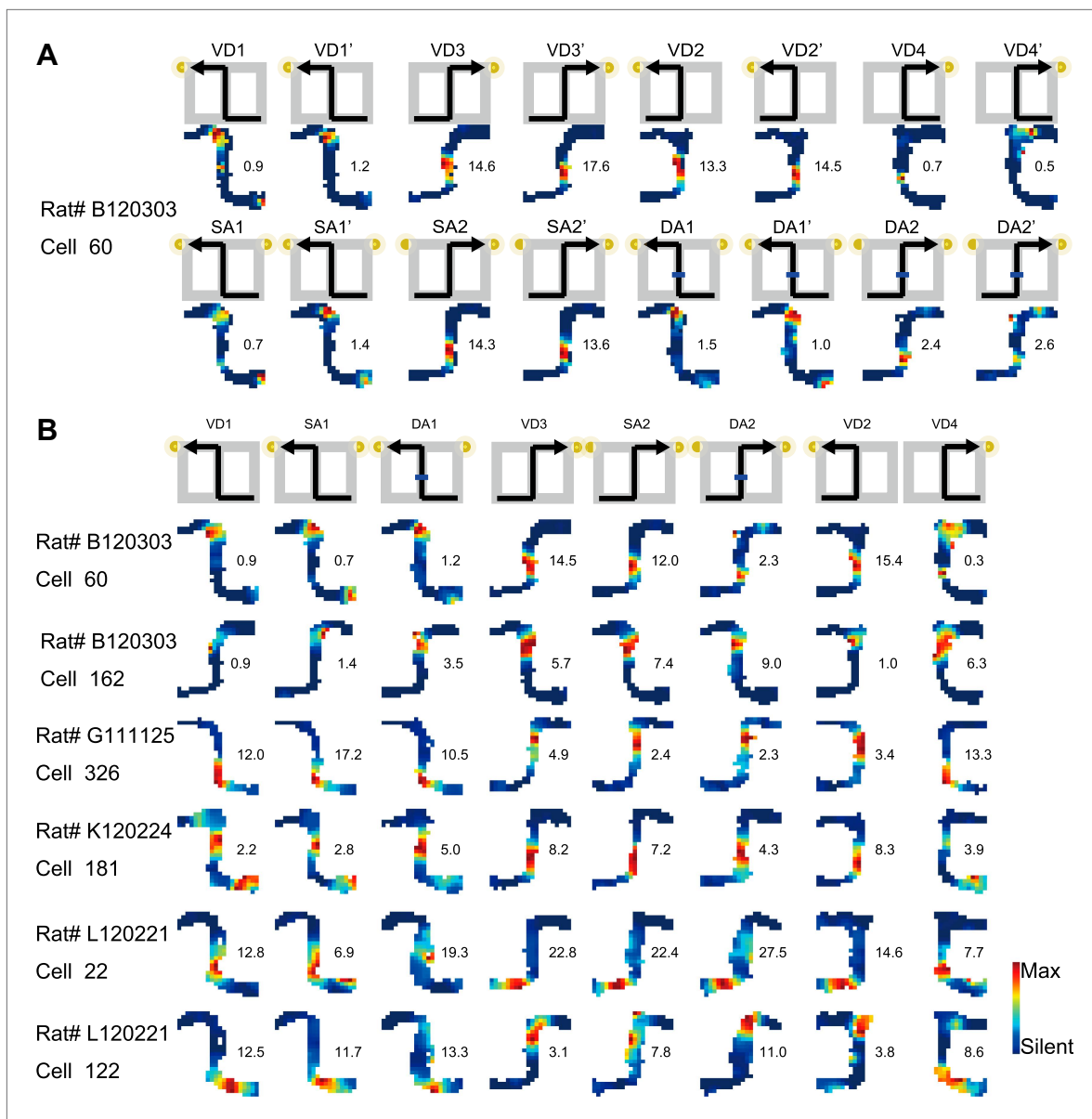


Figure 3. Journey-dependent coding of a place-specific activity modulated with task-demand. Representative color-coded rate maps for eight possible trial types. **(A)** The rate maps with the first cell in **(B)** show stable place-specific activity in repeated sessions of an identical journey within a given task-demand. The rate was coded on a color scale from blue (silent) to red (maximum rate). The pixels that were not sampled are white. The symbols above the map indicate the journey, task-demand and illuminated light-cue. For each cell, the rate scale corresponds to the peak firing rate in Hz in that condition (indicated to the right of the rate maps). **(B)** The rate maps for six CA1 pyramidal cells. The maps are averages for repeated sessions. Each row shows the data from one pyramidal cell. Note that different journeys in the same place resulted in place fields similar in locations, but different task-demands caused different firing intensities in those place fields.

DOI: [10.7554/eLife.00321.006](https://doi.org/10.7554/eLife.00321.006)

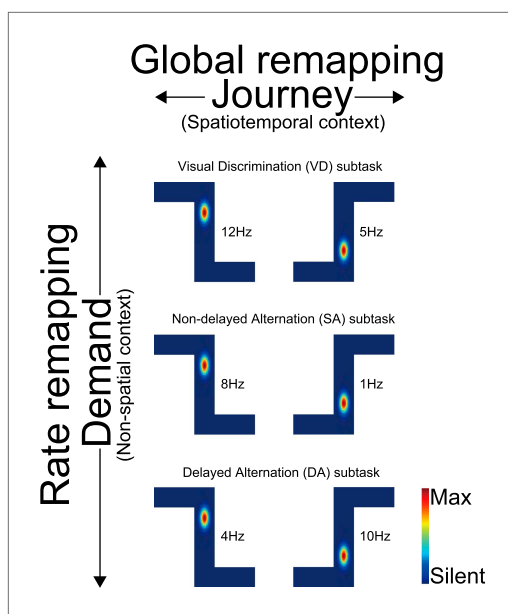


Figure 3—figure supplement 1. Schematic of the main finding with regard to place fields. A schematic showing remapping of the place fields that occurred between journeys (spatiotemporal contexts) and task-demands (non-spatial contexts) at the single cell level. Changes in both firing location and rates in the place field (global remapping) occurred between the different journeys. By contrast, only changes in the firing rates (rate remapping) occurred between the task-demands.

DOI: [10.7554/eLife.00321.007](https://doi.org/10.7554/eLife.00321.007)

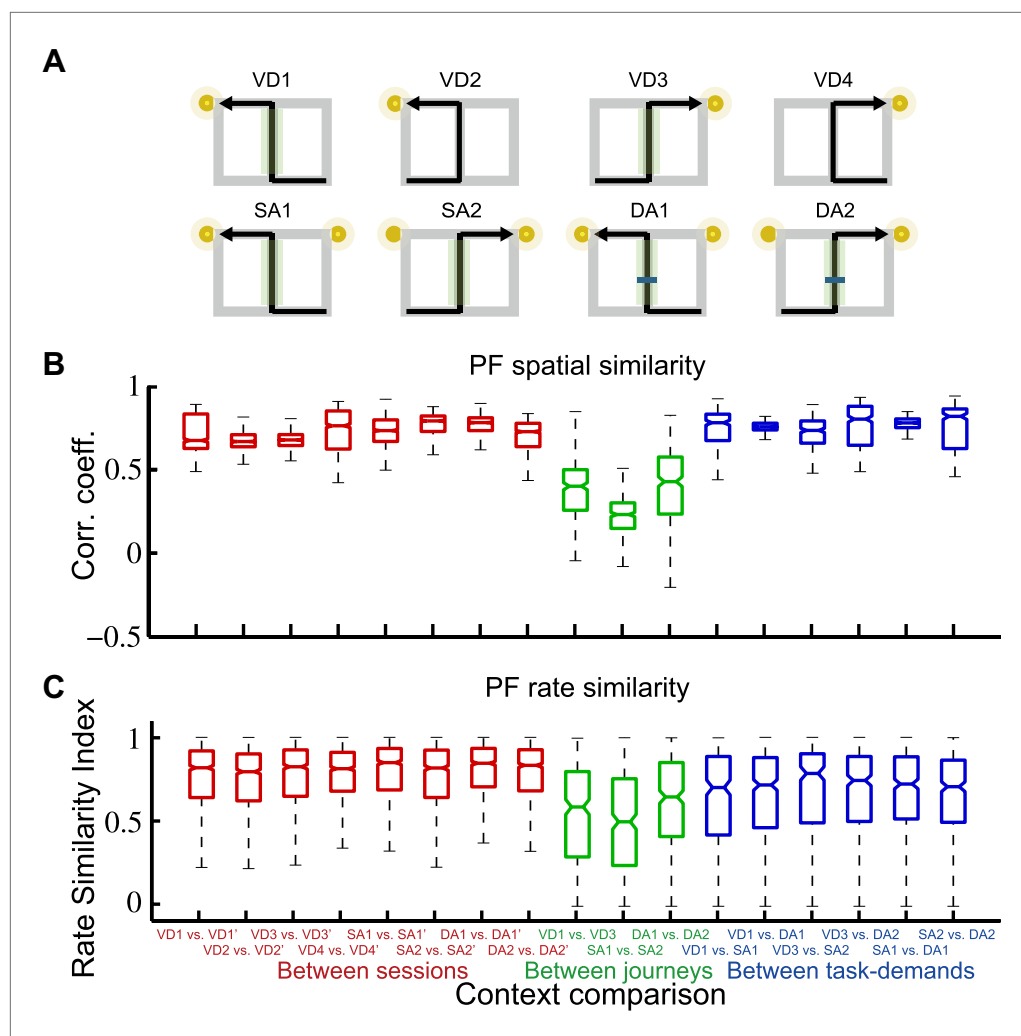


Figure 4. A quantitative assessment of the spatial and rate similarities between a pair of trial types. (A) The similarities were measured between a pair of trial types (VD1, VD2, VD3, VD4, SA1, SA2, DA1, and DA2) or between repeated exposures to an identical trial type. Because the central stem of the maze was the common running route among the different journeys within a given subtask, the region of interest (ROI) was set at the region highlighted in the green shaded box. Box plots of the spatial (B) and rate (C) similarities between repeated exposures to an identical journey and task-demand (red), between different journeys within a given task-demand (green), and between different task-demands within a journey (blue) (median, first and third quartiles, minimum, and maximum indicated). Repeated exposures are marked with an apostrophe.

DOI: [10.7554/eLife.00321.008](https://doi.org/10.7554/eLife.00321.008)

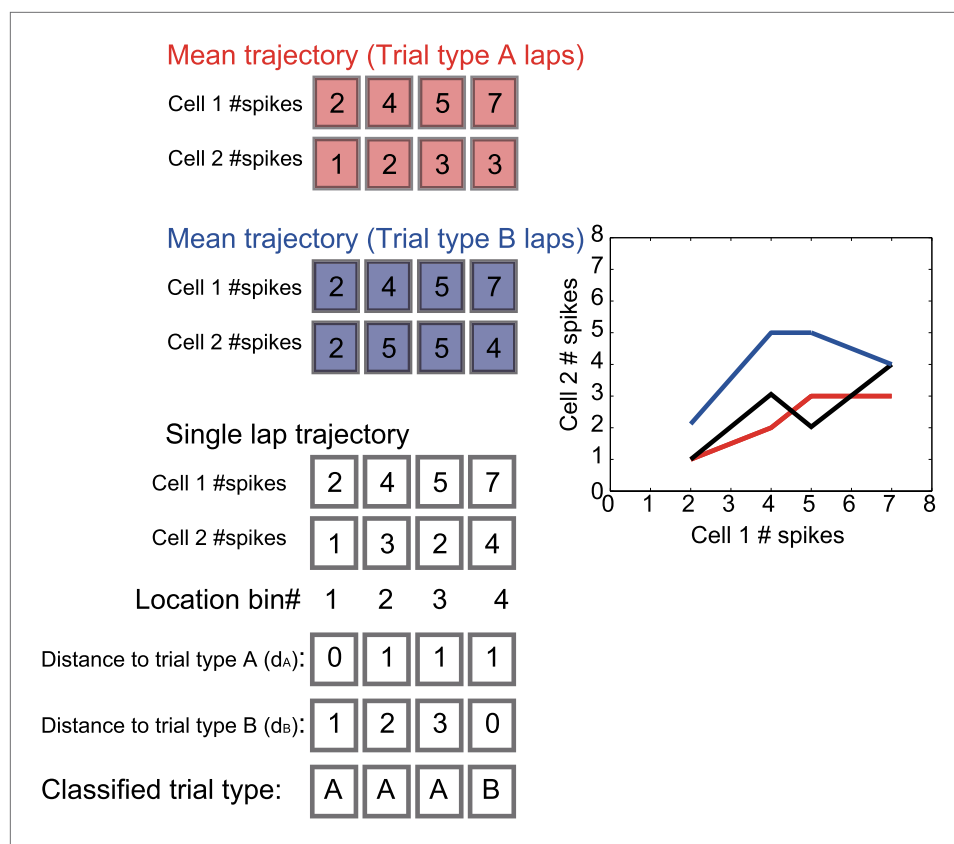


Figure 5. A schematic of a classification scheme based on the distances to the mean trajectories. At each location, the Euclidian distance from the trajectory on a single lap (black) to the mean trial type trajectories (red and blue) was calculated (d_A , d_B). If d_A was less than d_B , the lap at the location bin was classified as trial type A, and vice versa for trial type B.

DOI: [10.7554/eLife.00321.009](https://doi.org/10.7554/eLife.00321.009)

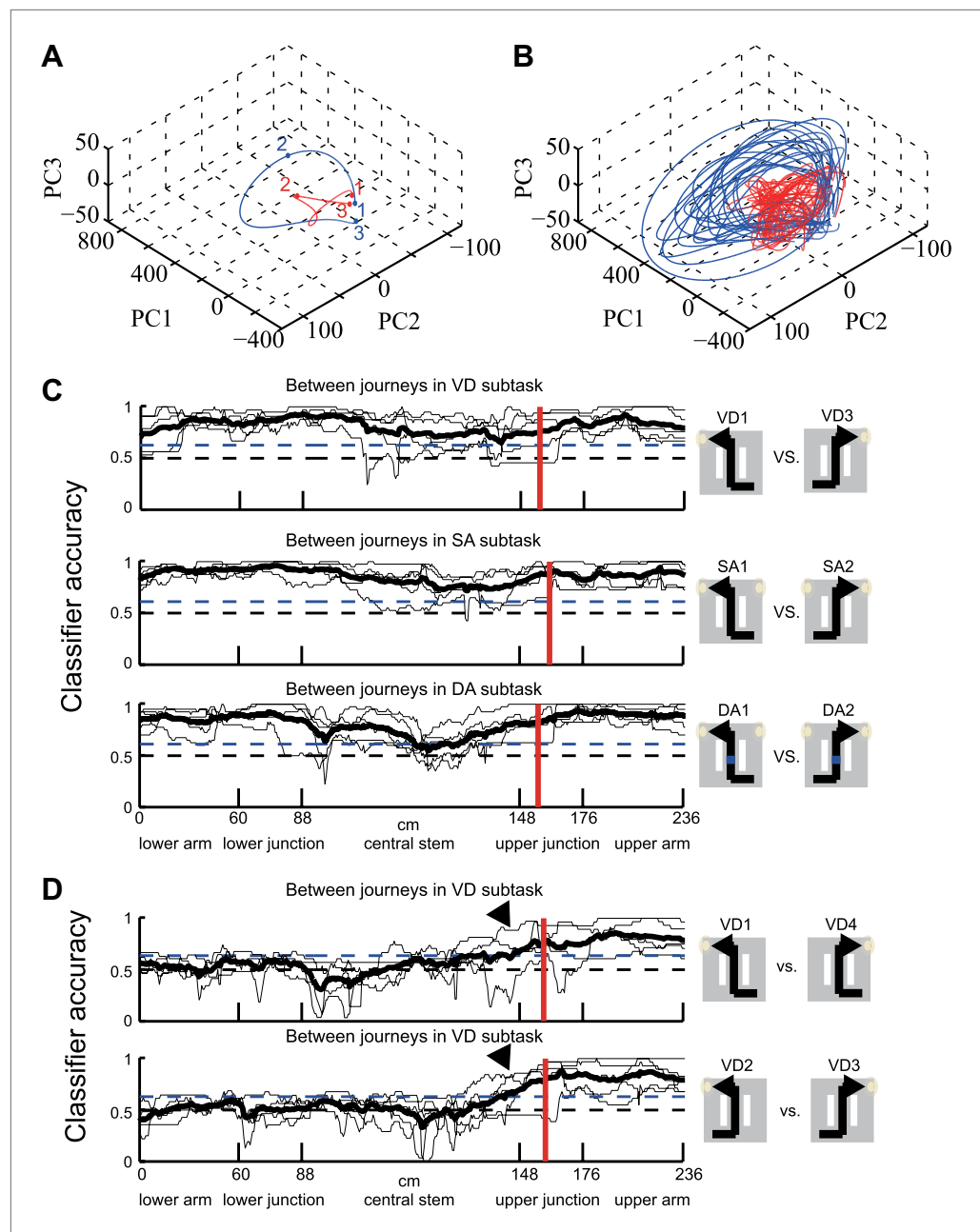


Figure 6. Neuronal trajectory of different journeys and different future directions. **(A)** An example time course of mean, journey-specific trajectories for right-to-left (red) and left-to-right (blue) laps in the SA subtask, plotted on the first to third principal component space (Rat #: B120303, $n = 91$ cells). The points marked 1, 2 and 3 correspond to the mean locations where the rat entered the lower arm, and turned and entered the reward zone, respectively. **(B)** Example individual trajectories for laps in the subtask in **(A)**. **(C)** The classification accuracy of determining the journeys (shown in right) at different locations in the VD, SA, and DA subtasks (thin black line, $n = 5$ rats; solid black line, mean; blue dashed line, $p = 0.001$, binomial test; black dashed line, chance level; red vertical line, mean turn onset). The classifier was based on a distance-dependent classification scheme. **(D)** As **(C)**, except that the subtask condition under which the future direction is not predictable until arriving at the decision point. A high level of accuracy can be observed even before the onset of the turn (arrow heads).

DOI: [10.7554/eLife.00321.010](https://doi.org/10.7554/eLife.00321.010)

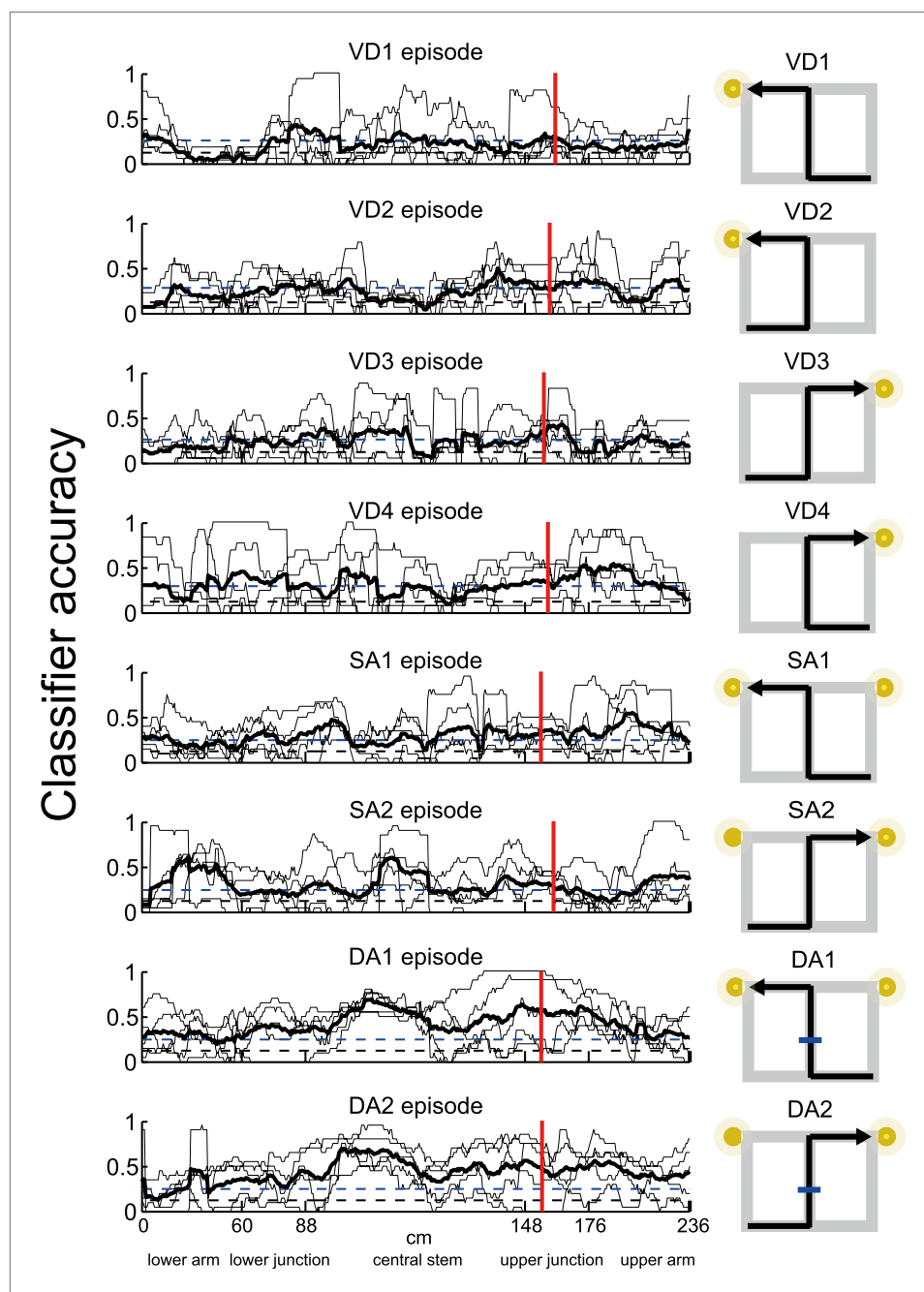


Figure 7. Episode-specific neuronal trajectories. The classification accuracy for determining a trial type from all of the possible trial types (episodes) (thin line, $n = 5$ rats; thick black line, mean; blue dashed line, $p=0.001$, binomial test; black dashed line, chance level). The classifier was based on a distance-dependent classification scheme. The average accuracy for each rat was significantly higher than chance at the respective specific locations.

DOI: [10.7554/eLife.00321.011](https://doi.org/10.7554/eLife.00321.011)

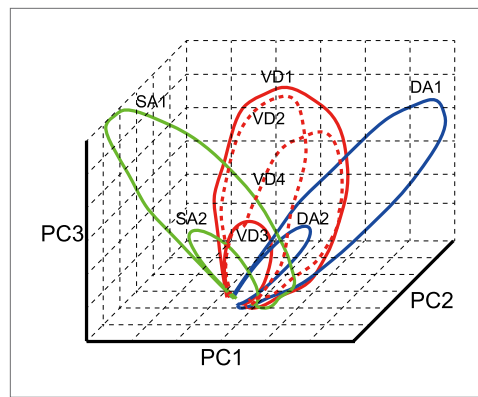


Figure 7—figure supplement 1. Schematic of the main finding with regard to episode-specific neuronal trajectories. A schematic of the hypothetical, episode-specific neuronal trajectories of an individual trial type (red lines: VD subtask, green lines: SA subtask, blue lines: DA subtask; red dashed lines: same origin and destination) in the first to third PC space. As expected from the place field properties, the same right-to-left/left-to-right journey produces a similar neuronal trajectory at the ensemble level. However, the trajectories are shifted between the task-demands in certain spaces (PC2 in this schematic), thereby generalizing a journey over task-demands. When the future direction changes from the expectation at the decision point, the trajectory shifts to the corresponding one (red dashed lines, VD2, VD4). The trajectory shift can be triggered not only by external events (the light-cues) but also by internal events (expected future direction) before the behavioral choices.

DOI: [10.7554/eLife.00321.012](https://doi.org/10.7554/eLife.00321.012)

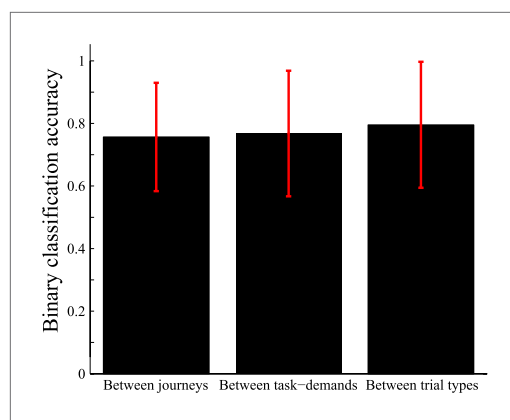


Figure 8. Comparison of accuracy of distinguishing journeys, task-demands and trial types from neuronal ensemble activity. Average binary classification accuracies of distinguishing pairs of journeys (i.e., VD1, SA1, and DA1 vs VD3, SA2, and DA2), pairs of task-demands (i.e., VD vs SA, VD vs DA, and SA vs DA), and pairs of trial types (i.e., all possible pairings of VD1, VD2, VD3, VD4, SA1, SA2, DA1, and DA2). For each rat, the accuracy was calculated based on the most frequently classified choices in the central stem. The error bars indicate SD.

DOI: [10.7554/eLife.00321.013](https://doi.org/10.7554/eLife.00321.013)

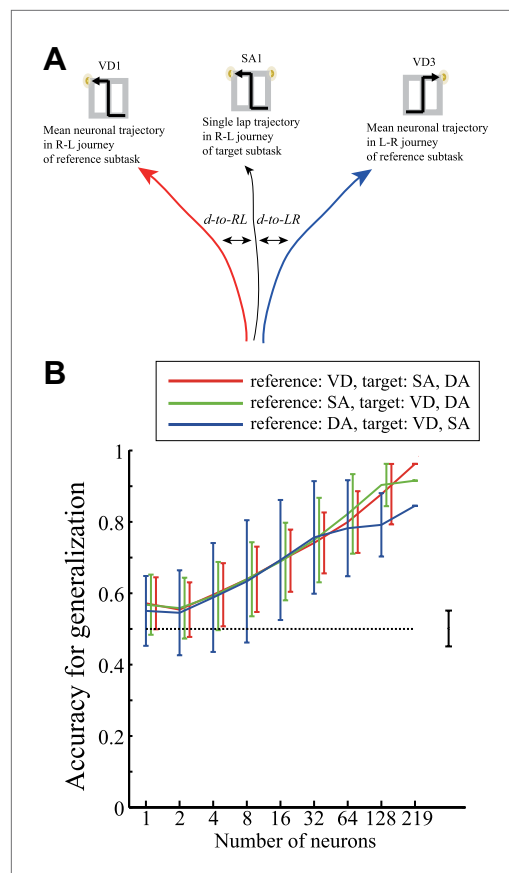


Figure 9. Generalization accuracy of determining a journey over task-demands from neuronal ensemble activity. **(A)** Schematic of a classification scheme for estimating generalization accuracy. At each location, the distance from the trajectory in two target subtasks on a single trial to the mean right-to-left (R-L) and left-to-right (L-R) journey trajectories in a reference subtask was measured ($d\text{-to-RL}$ and $d\text{-to-LR}$). If the actual journey was R-L, and $d\text{-to-RL}$ was less than $d\text{-to-LR}$, the lap at that location was classified as a correct generalization, and vice versa. The figure shows an example in which a reference subtask is VD and a neuronal trajectory in the R-L journey of an SA subtask was examined. **(B)** The generalization accuracy for determining a R-L/L-R journey from the neuronal trajectory in each lap in two of the three subtasks based on the distance to the mean neuronal trajectories in a remaining reference subtask as a function of the number of cells (red: reference: VD, target: SA and DA; green: reference: SA, target: VD and DA; blue: reference: DA, target: VD and SA). Cells recorded from five rats were combined. The accuracy was calculated based on the most frequently classified journeys in the central stem. The error bars show the SD for 1000 random choices of the cells used; the dashed line shows the chance level, and the bar next to the dashed line shows the range of accuracies using random shuffling (control).

DOI: [10.7554/eLife.00321.014](https://doi.org/10.7554/eLife.00321.014)